The Astrophysical Journal, 632:499–503, 2005 October 10

SPIRAL PATTERNS AND SHOCKS IN LOW-COMPRESSIBILITY ACCRETION DISKS AROUND COLLAPSED OBJECTS: TWO-DIMENSIONAL SPH MODELING

G. Lanzafame[1] and G. Belvedere[2]
Received 2005 February 16; accepted 2005 June 18

ABSTRACT

In recent years contrasting results have been found regarding the onset of spiral structures and shock fronts in accretion disks around compact objects. Indeed, according to some authors, spiral structures and shock fronts do not develop if an adiabatic index $\gamma > 1.16$ is adopted. On the contrary, other authors obtain well-developed spiral patterns and shocks adopting $\gamma = 1.2$. In this paper, by using a smoothed particle hydrodynamics (SPH) code, we show that clear spiral patterns and strong radial shocks come out even in very low compressibility ($\gamma = 1.3 > 1.16$) accretion disk models in close binaries if the primary is a massive black hole (MBH) with a mass 30–60 times larger than the secondary, whatever the geometrical and dynamical conditions at the inner Lagrangian point, L1, may be, independent of sonic or subsonic injection flow boundary conditions. Indeed, the rationale of this work is that in close binary systems in which the primary is a MBH and the secondary is a low-mass star, we have enough initial energy and angular momentum at the inner Lagrangian point, L1, and a wide and deep enough primary potential well to favor the development of well-defined spiral structures, and eventually spiral shocks, independent of the gas compressibility. According to our results the presence of a MBH triggers the development of spiral structures and spiral shock fronts in the accretion disk both at its outer edge and in the disk bulk, because of the high particle concentration and the strong collisions induced by the strongly accelerated stream particles with the high initial angular momentum at L1.

Subject headings: accretion, accretion disks — binaries: close — black hole physics — methods: numerical — shock waves

1. INTRODUCTION

In accretion disk modeling, it is remarkably helpful to study the hydrodynamic regime by simulating the radiative cooling with an adopted value for the ratio of specific heats, γ. This is an active research field to which several papers have contributed in recent years. The onset and development of spiral structures and shock fronts are also of great interest in accretion disk modeling in close binary systems, inasmuch as they are responsible for dominant dynamical and energetic effects, such as gas heating, gas outflows, and angular momentum transport. On the observational side, the existence of spiral density waves should in principle be revealed through the analysis of orbital phase–dependent prominent emission lines. The theoretical grounds of this method have been explored with great accuracy by Steeghs & Stehle (1999).

In recent years, a number of papers have been devoted to the problem of spiral pattern and spiral shock front formation in accretion disks around compact objects such as white dwarfs, neutron stars, and black holes, (e.g., Spruit et al. 1987; Kaisig 1989; Matsuda et al. 1990, 1992; Molteni et al. 1991; Chakrabarty 1992; Meglicki et al. 1993; Yukawa et al. 1997; Lanzafame & Belvedere 1997, 1998; Bisikalo et al. 1999; Steeghs & Stehle 1999; Blondin 2000; Lanzafame et al. 2000, 2001; Lanzafame & Belvedere 2001; Belvedere & Lanzafame 2002). In particular, Lanzafame et al. (2000, 2001) provide an analysis of spiral shock pattern features in a bidimensional parameter space, namely, as a function of the M_2/M_1 mass ratio and the angular momentum at L1.

Some of these papers have questioned whether spiral patterns and spiral shock fronts develop in accretion disks around compact objects, depending on the gas compressibility. Such papers disagree with one another about the conditions suitable to generate such spiral structures. In fact, some authors (Matsuda et al. 1990, 1992; Yukawa et al. 1997) claim that spiral structures emerge easily, due to small perturbations of the initial conditions, whatever the gas compressibility may be (e.g., whatever the adiabatic index γ may be), in both two-dimensional and three-dimensional simulations. According to Yukawa et al. (1997), only highly compressible (quasi-isothermal) three-dimensional accretion disk modeling prevents spiral structures from forming, because of the highly degrading effect of the artificial viscosity in the disk bulk. On the other hand, different authors (Chakrabarty 1992; Bisikalo et al. 1999) conclude that spiral structures do not develop if an adiabatic index $\gamma > 1.16$ is adopted.

Lanzafame & Belvedere (1997, 1998) found spiral structures in three-dimensional SPH accretion disk models around a compact primary in close binary systems by adopting an adiabatic index $\gamma = 1.01$. Then Lanzafame et al. (2000, 2001) singled out which geometrical and dynamical conditions at the inner Lagrangian point, L1, may support spiral pattern and shock development in two-dimensional highly compressible SPH disks with $\gamma = 1.01$, concluding that a low M_2/M_1 mass ratio and a high injection flow angular momentum at L1 favor the onset of spirals and radial shocks.

Moreover, Lanzafame & Belvedere (2001) and Belvedere & Lanzafame (2002) showed that well-developed spirals and shock fronts emerge even in low-compressibility (e.g., $\gamma > 1.16$) SPH two-dimensional disks, if the primary is a black hole. They performed two two-dimensional and two three-dimensional simulations, each pair comprising adopted adiabatic index $\gamma = 1.01$ and $\gamma = 1.3$ (high- and low-compressibility cases). Indeed, both two-dimensional models reveal the existence of spiral structures

[1] INAF—Osservatorio Astrofisico di Catania, Via S. Sofia 78, 95123 Catania, Italy; glanzafame@ct.astro.it.
[2] Dipartimento di Fisica e Astronomia dell'Universitá—Sezione Astrofisica, Via S. Sofia 78, 95123 Catania, Italy; gbelvedere@ct.astro.it.

in the disk bulk, and spiral shocks at the outer disk edge are evident for the high-compressibility two-dimensional model. Spiral structures appear to develop even for the three-dimensional high-compressibility model. However, for the three-dimensional low-compressibility model, no clear conclusion can be drawn because of the lack of resolving power.

In all of these SPH simulations, artificial viscosity is introduced to resolve shocks numerically and to avoid spurious heatings and discontinuities. The artificial viscosity is responsible for mass and angular momentum transport and vanishes when the particle interpolation domain goes to zero. The smoothing effects of the artificial viscosity are weaker in two-dimensional than in three-dimensional models (Monaghan 1992; Monaghan & Lattanzio 1985).

In this paper, by using a typical SPH code that is a highly implemented version of Monaghan's original one, we show that evident spiral patterns and strong radial shocks emerge even in low-compressibility ($\gamma = 1.3$) accretion disk models if the primary component is a MBH with a mass 30–60 times larger than that of the secondary, whatever the geometrical and dynamical initial boundary conditions at L1 may be.

In fact, the rationale of this work is that in close binary systems in which the primary is a massive collapsed object (i.e., not a white dwarf or a neutron star, but necessarily a MBH) and the secondary is a low-mass star, we have enough initial energy and angular momentum at L1 (and a wide and deep enough primary potential well) to favor the development of well-defined spiral structures, and eventually spiral shocks, independent of the gas compressibility. Indeed, we simulate an accretion disk around a massive compact primary whose potential well is deep enough to concentrate particles despite the gas pressure $\propto(\gamma - 1)$. Indeed, the gas pressure is given by the state equation $p = (\gamma - 1)\rho\epsilon$, where ϵ is the thermal energy per unit mass. A simple order of magnitude estimate predicts that if we typically find spirals for a disk with $\gamma = 1.01$ around a 1 $M_\odot$ white dwarf, we need at least a 30 $M_\odot$ MBH in order to develop spirals of comparable properties with $\gamma = 1.3$. This is because the ratio of gas pressure forces to gravitational forces is more or less the same. However, different disk characteristics should be expected in the MBH case, since the initial particle acceleration at L1 is much stronger.

It must be remarked that in calculations such as those in this paper, adopting a ratio of specific heats lower than those in the adiabatic case ($\gamma = 5/3$) means that the effect of radiative cooling is simulated. In principle, one cannot arbitrarily define the value of γ. Here we refer explicitly to the analysis performed by Sato et al. (2003). However, it is not an easy task to estimate the value of γ for a disk around a MBH. In all usual simulations (especially the ones we refer to) γ is a free parameter, and all previous studies of this kind explored the possibility of the onset of spiral shocks in terms of the ratio between specific heats. Some authors found shocks for low-compressibility disks, while others did not. In this work we show that shocks take place, even for $\gamma = 1.3$, if the central object is a MBH. The work by Sato et al. (2003) shows, under various approximations, that the effect of radiative cooling is best simulated by adopting $\gamma < 1.1$, but does not exclude larger values of γ, for instance, $\gamma = 1.2$. Indeed, it is reasonable to believe that γ-values between 1.01 and 1.3 simulate the radiative cooling fairly well.

On the other hand, it is well known that $\gamma = 1.01$ corresponds to the nearly isothermal case, so it is not surprising that Sato et al. (2003) find no radial temperature gradient for $\gamma = 1.01$. Indeed, they consider a radiative transfer only in the direction vertical to the disk plane. The lack of a radial temperature gradient is compatible with a low-mass central object, as in Sato et al. (2003).

However, for a very deep potential energy well such as that considered in our work, in which the MBH mass is as large as 32 $M_\odot$, a strong radial temperature gradient is expected as a consequence of the fast increase of the radial kinetic energy of particles. Of course, a radial temperature gradient larger than zero corresponds to a γ larger than the unity. Therefore, on the basis of this qualitative argument, γ-values such as 1.2–1.3 should be compatible with the strong radial temperature gradient associated with a MBH. Furthermore, it is obvious that if we adopted lower values for γ with a central object of such large mass, spiral shocks would appear a fortiori, since the gas compressibility would increase. Note that the appearance of spiral shocks for $\gamma = 1.01$ has already been shown by Belvedere & Lanzafame (2002) for a much smaller black hole mass (8 $M_\odot$) and the same secondary mass (0.5 $M_\odot$).

Finally, in our model the effect of the tidal forcing is negligible. Of course, the tidal term is included in the expression for the gravitational potential, but it can be neglected, since the mass ratio M_2/M_1 is very small ($M_2/M_1 \simeq 0.015$) in comparison, e.g., with Blondin (2000), whose lowest mass ratio is 0.2. Therefore, in the present simulation, spiral structures develop only because of the impact of the accreting stream toward the disk edge, in the framework given above.

2. MODEL PARAMETERS AND BOUNDARY CONDITIONS

The binary system characteristics are determined by the masses of the two companions—$M_1 = 32\ M_\odot$, the MBH primary, and $M_2 = 0.5\ M_\odot$, the red subgiant secondary star—and by the separation between their centers, $d_{12} = 10^8$ km. The injection gas velocity at L1 is $v_{\rm inj} \simeq 15$ km s^{-1}, very close to the sound velocity, while the injection gas temperature at L1 is $T_0 = 10^4$ K, a value slightly higher than usual, since we take into account the radiative heating of the secondary surface by the disk. The adopted adiabatic index is $\gamma = 1.3$, as in Lanzafame & Belvedere (2001) and Belvedere & Lanzafame (2002).

The large number of particles in a MBH deep potential well, even for a high γ-value, allows a good resolving power and reliable statistics, even if the degrading effect of the artificial viscosity on shock fronts is stronger in the disk bulk. Nevertheless, in such conditions, shock fronts are strong enough to appear.

We reiterate the physical meaning of our parametrization in terms of the adiabatic index γ. We have four unknowns—pressure, density, temperature, and velocity—so we need to solve four equations: continuity, momentum, energy, and state (perfect gas). The state equation for a polyatomic perfect gas is $p = (\gamma - 1)\rho\epsilon$. Thus, the adiabatic index γ has the meaning of a physical parameter, which in principle ranges between 1 and 5/3.

In order to make the equations dimensionless, we adopted the following normalization factors: $M = M_1 + M_2$ for masses, $d_2 = 10^{13}$ cm for lengths, and $v_0 = [G(M_1 + M_2)/d_{12}]^{1/2}$ for velocities, so the orbital period is normalized to 2π, $\rho_0 = 10^{-9}$ g cm^{-3} for the density, $p_0 = \rho_0 v_0^2$ dyn cm^{-2} for the pressure, v_0^2 for the thermal energy per unit mass, and $T_0 = (\gamma - 1)v_0^2 m_p k_{\rm B}^{-1}$ for the temperature, where m_p is the proton mass and $k_{\rm B}$ is the Boltzmann constant.

The kernel width in the SPH interpolations is $h = 0.005$, and the geometrical domain, which comprises the moving disk particles, is a sphere of radius 1, centered at the primary. The adopted h-value allows us to perform reasonably good SPH interpolations. In fact, the particle concentration, even in the more rarefied zones inside the primary Roche lobe, is high enough to allow each particle to be surrounded by at least 20 other particles, while in the injected dense particle stream each particle is surrounded by more

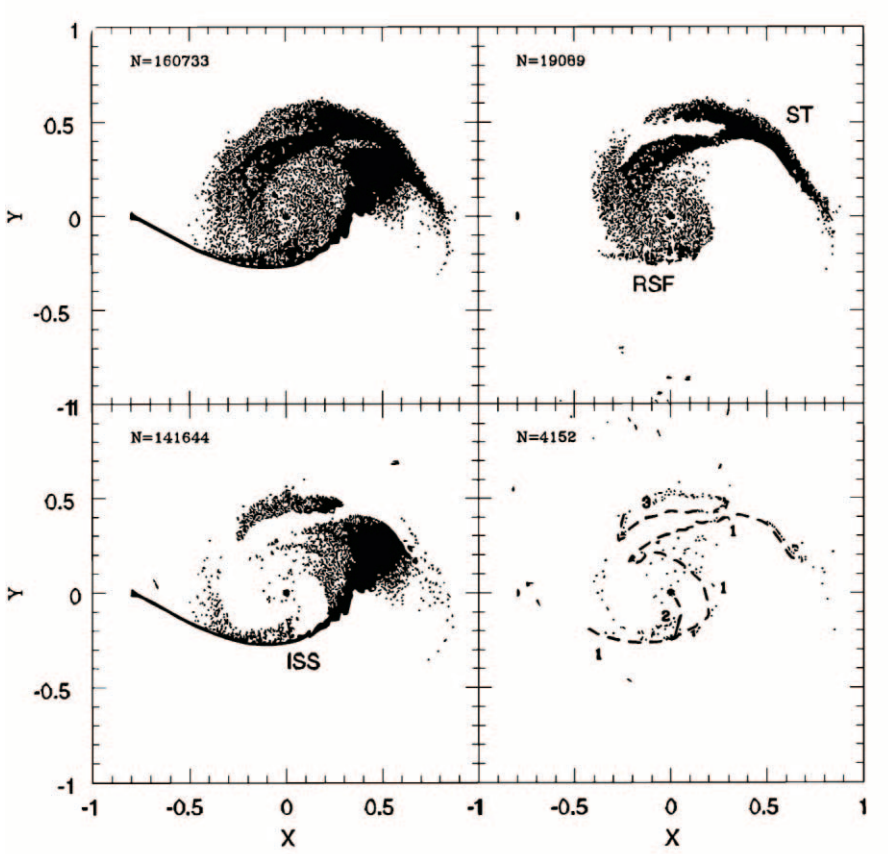

FIG. 1.—(X, Y) plots showing all particles (*top left panel*), the radial flow subsonic component only (*top right panel*), the supersonic component only (*bottom left panel*), and the radial shock fronts (*dashed lines*) together with the particle component whose radial Mach number is $0.95 \leq \mathcal{M}_r \leq 1.05$ (*bottom right panel*). The total number of particles N is reported. For the sake of clarity, the incoming supersonic stream (ISS), the subsonic tail (ST), and the returning subsonic flow (RSF) are indicated. The shock fronts are labeled 1, 2, and 3.

than 100 particles. The rotating reference frame is centered at the primary, and its rotational period equals the orbital period. We simulated the physical conditions at the inner and outer edges as follows:

Inner edge.—The free inflow condition is realized by eliminating particles flowing inside the sphere of radius $4h$, centered at the primary. It follows that the disk structure and dynamics are altered a few h values near the inner edge by adopting a fixed h SPH code, but these modifications are small because they are compensated by a good particle concentration close to the inner edge in the supersonic injection models.

Outer edge.—The injection of "new" particles from L1 toward the interior of the primary Roche lobe is simulated by generating them in fixed points, called "injectors," symmetrically placed within an angle having the L1 point as a vertex and an aperture of $\sim 57^\circ$. The initial injection particle velocity is radial with respect to L1. In order to simulate a constant and smooth gas injection, a "new" particle is generated in an injector whenever "old" particles leave the injector free inside a small spherule with radius h, centered at the injector itself. The primary Roche lobe was assumed to be empty at time $t = 0$. This is a common configuration, widely adopted by various authors. On the other hand, it is impracticable to assume different initial conditions, in particular if a non-Keplerian gas dynamics has to be taken into account.

3. RESULTS AND DISCUSSION

We carried out our simulation far enough to get a fully stationary configuration in which particle injection from L1 statistically balances particle accretion from the inner edge and particle ejection from the outer edge. In practice we carried out our calculations for about two orbital periods. Then we decided to stop them, since we had attained a fully stationary state with a huge total number of disk particles (160,733).

Note that the shock patterns we find are not generated by small initial (but nonpersistent) perturbations at the disk outer edge (typically tidal forces or negligible collisional perturbations originated from the stream impact), but arise from the strong supersonic flow originating at L1 and are subject to the huge gravitational attraction exerted by the MBH in the whole course of the disk evolution. In this sense, it would be correct to speak of a kind of close connection between the strong incoming stream and the disk itself: they seem to be a single body. The violent injected stream limits the disk's radially symmetric expansion from the impact side. A similar situation has been simulated, although in a different context, by Lanzafame et al. (1993) for the active phase of SS Cyg, for which they introduced the so-called belt effect. This barrier phenomenon, present since the initial phases of mass transfer, prevents the disk from radial expansion. Therefore, a wide portion of the primary Roche lobe would be permanently forbidden to the forming disk, and the disk itself would be permanently asymmetric. As a natural consequence, this disk's permanent asymmetry gives rise to (but does not contrast with) strong shock fronts. Therefore, after about two orbital periods the disk is well defined, and its structure and characteristics seem to be stable and consolidated; in particular, the onset of spiral patterns and shocks is clearly evident.

Several relevant results are shown in Figure 1, which describes the two-dimensional accretion disk structure and dynamics. In this

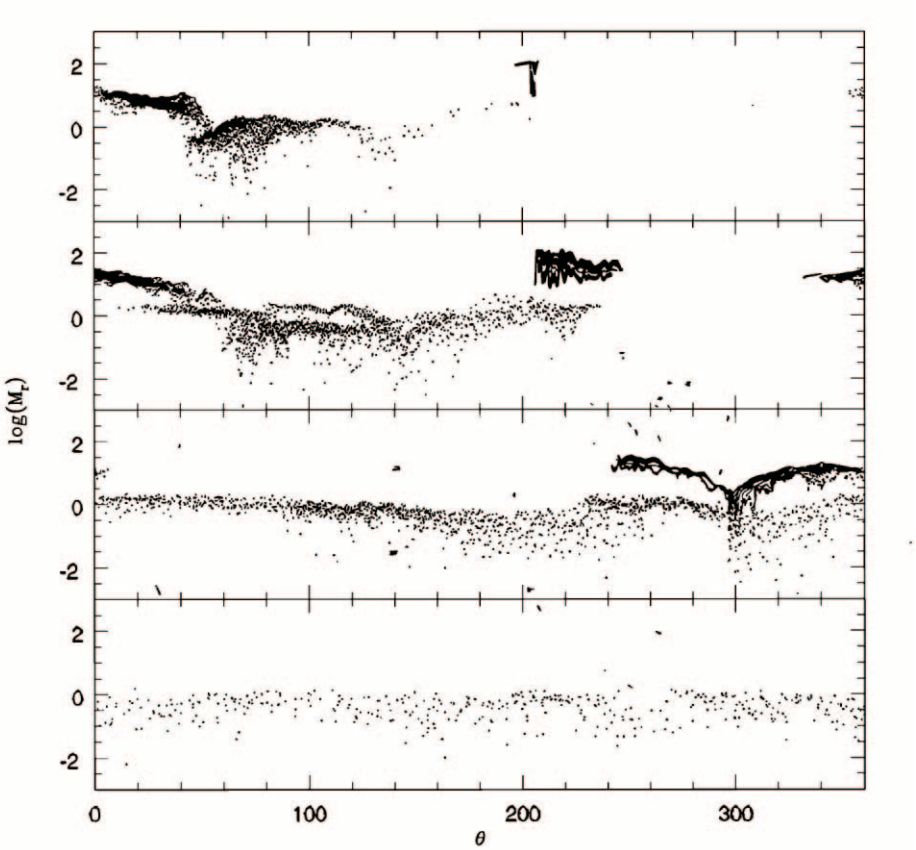

FIG. 2.—Azimuthal distribution of the radial Mach number $\mathcal{M}_r$ in a semilogarithmic scale for four radial distance (r) shells. Particles with $r \leq 0.15$ are reported in the bottom diagram. Particles with $r \geq 0.45$ are reported in the top diagram. Each shell has a thickness $\Delta r = 0.15$. The radial distance r increases from the bottom to the top.

figure both subsonic and supersonic disk radial components of the velocity field are also shown.

We realize that gravitational forces dominate over gas pressure, starting from the phase of injection of particles at L1. In fact, notwithstanding the high $\gamma = 1.3$ adopted here (low compressibility), the injected particles are strongly compressed in a thin, well-defined, highly supersonic incoming stream. This means that the disk structure and dynamics are ruled by the primary gravitational field and by the supersonic collisional push of the injected stream particles. As a consequence, the disk shows evident asymmetries both at its outer edge and in its bulk, as shown in Figure 1: the whole disk is about twice as elongated in the direction going from the region where the stream particles collide with the disk outer edge up to the opposite side. Moreover, powerful collisions at the disk outer edge generate strong turbulences in the terminal portion of the incoming supersonic stream (ISS) on the opposite side. The disk outer edge elongation and these turbulences are strictly connected with each other as a consequence of the huge push exerted by the ISS onto the subsonic tail (ST), which is the dominant structure in the extended outer edge. The ST appeared at the initial phases of disk formation. In fact, the ISS is slung away from the MBH and slowed because of the artificial viscosity dissipation. The onset of very strong spiral shocks is evident in Figure 1 looking both at the overall disk particle distribution and at its supersonic or subsonic components. Moreover, a dashed line in the bottom right panel of Figure 1 allows us to distinguish three clear shock fronts. The first and more elongated of them (No. 1) originates directly from collisions of the ISS both with the returning subsonic flow (RSF), which has completed a full turn around the primary, and with the ST at the outer edge. The second and shorter shock front (No. 2) is a small branch that does not originate from the first one, as might be interpreted from the bottom right panel of Figure 1, but rather is ascribed to the spiral supersonic flow extracted from the ISS because of the angular momentum loss in particle collisions with the RSF (see also Fig. 1, *bottom left panel*). The third and last shock front (No. 3) originates from the gravitationally accelerated supersonic particle flow coming from the ST and then colliding with the subsonic bulk.

The existence of remarkably strong spiral shocks is also confirmed by Figure 2, in which four particle azimuthal distributions of the radial Mach number are reported for four radial distance shells as thick as $\Delta r = 0.15$. Here the azimuthal angle θ is counted counterclockwise from the X-axis, oriented from the secondary to the primary. This diagram shows once more that spiral shocks exist in particular for radial distances $r > 0.15$, and that spiral shocks occurring within the azimuthal field $205^\circ < \theta < 360^\circ$ are related to the injected supersonic flow coming from L1, while those occurring within the azimuthal field $0^\circ < \theta < 50^\circ$ are related to the collisional interaction of the terminal segment of the supersonic turbulent stream with the disk outer edge. Other weaker spiral shocks, such as those occurring close to the outer edge within the azimuthal field $80^\circ < \theta < 130^\circ$, are related to the particle supersonic flow originating from the ST previously discussed.

From these synoptic plots it is clear that the onset of the spiral shock pattern is to be attributed to the impact of the incoming supersonic stream on the disk edge since the initial phases of the disk lifetime. From these plots it is also evident that the spiral shock area increases with time, and eventually a subsonic tail

begins to form. These are not transient phenomena that may be attributed to the lack of circularization of orbits, but rather enduring ones caused by the strong impact of the incoming supersonic flow, which evidently persist for the entire disk lifetime. In addition, the elongated disk shape is not due to the lack of circularization, but is a consequence of the violent impact. Moreover, we calculated the tangential (Keplerian) Mach number $\mathcal{M}_t = V_k/C_s$ and found low values (0.75–1) in the subsonic tail, which indicate an open spiral pattern. This is in agreement with the elongated external disk structure. In the shock region, we find higher values (15–20), which indicate a tighter spiral pattern; this is in agreement with the more circular internal disk structure. We want to stress that the onset (and the permanence) of spiral shock patterns and the inflowing supersonic stream are intimately connected with each other. The turning off of the mass transfer process extinguishes spiral shocks and, in a short time afterward, the overall disk structure itself, because of the mass and angular momentum viscous transport. A large part of the outer disk edge is made up of the huge supersonic inflowing stream coming from L1 and the outflow coming from the disk bulge due to angular momentum transport. In particular, in two dimensions, this second flow is prevented from further outflowing toward deep space because of the supersonic injected inflow at the disk outer edge wall, where the two flows heavily collide. On the other hand, we have already said that after about two rotational periods statistical equilibrium is reached, and then the disk becomes stationary. The number of particles constituting the disk remains constant in time, and the disk can no longer change its structure and dynamics. In this situation, on average, all new particles generated in the injectors will be directly accreted to the MBH. Indeed, our numerical simulation shows that, after about two rotational periods, both the injection and accretion rates are about 10^{20} g s^{-1}, while the ejection rate (number of particles per unit time added to the disk or dispersed into deep space) is very negligible. This is a situation of dynamical equilibrium in the presence of the supersonic injection stream. Suppose we turn off the tap. In the absence of feeding, one can estimate that shocks would smooth out due to the presence of viscosity η, on a timescale $t_{\rm visc} \simeq R^2_{\rm spiral}/\eta$ (here $R_{\rm spiral}$ is the spiral shock characteristic scale length, very close to the disk radius $R_{\rm disk}$) of the order of 4 yr. However, the disk itself would be swallowed up by the MBH on a shorter timescale, of the order of $R_{\rm disk}/v_{\rm radial} \simeq$ 1 yr at most. But this is not a real astrophysical situation, since the injection proceeds on a timescale of the order of 2.5×10^{12} s $\simeq$ 10^5 yr (secondary envelope mass/injection rate).

Therefore, our present results together with the arguments and results given in Lanzafame & Belvedere (2001) and Belvedere & Lanzafame (2002) allow us to conclude that no spirals develop in low-compressibility accretion disk SPH models if the accretor is a white dwarf or a neutron star. Indeed, for high values of γ, spiral patterns and radial shocks can form only if the primary is a BH, and especially if it is a MBH. These results are better enhanced in two-dimensional models. In fact, three-dimensional models and, in particular, three-dimensional SPH models, are not suitable to study this problem, because the artificial viscosity shock smoothing effect is stronger than that in two-dimensions. On the other hand, three-dimensional accretion disk models with a MBH as a primary would require a huge CPU time in order to perform reliable simulations.

REFERENCES

Belvedere, G., & Lanzafame, G. 2002, PASJ, 54, 781
Bisikalo, D. V., Boyarchuk, A. A., Chechetkin, V. M., Kutznetsov, O. A., & Molteni, D. 1999, Astron. Rep., 43, 797
Blondin, J. 2000, NewA, 5, 53
Chakrabarty, S. K. 1992, MNRAS, 259, 410
Kaisig, M. 1989, A&A, 218, 102
Lanzafame, G., & Belvedere G. 1997, MNRAS, 284, 957
———. 1998, MNRAS, 295, 618
———. 2001, J. Korean Astron. Soc., 34, 313
Lanzafame, G., Belvedere, G., & Molteni, D. 1993, MNRAS, 263, 839
Lanzafame, G., Maravigna, F., & Belvedere, G. 2000, PASJ, 52, 515
———. 2001, PASJ, 53, 139
Matsuda, T., Ishii, T., Sekino, N., Sawada, K., Shima, E., Livio, M., & Anzer, U. 1992, MNRAS, 255, 183
Matsuda, T., Sekino, N., Shima, E., Sawada, K., & Spruit, H. 1990, A&A, 235, 211
Meglicki, Z., Wickramasinghe, D., & Bicknell, G. V. 1993, MNRAS, 264, 691
Molteni, D., Belvedere, G., & Lanzafame, G. 1991, MNRAS, 249, 748
Monaghan, J. J. 1992, ARA&A, 30, 543
Monaghan, J. J., & Lattanzio, J. C. 1985, A&A, 149, 135
Sato, J., Sawada, K., & Ohnishi, N. 2003, MNRAS, 342, 593
Spruit, H. C., Matsuda, T., Inoue, M., & Sawada K. 1987, MNRAS, 229, 517
Steeghs, D., & Stehle, R. 1999, MNRAS, 307, 99
Yukawa, H., Boffin, H. M. J., Matsuda, T., & Inoue, M. 1997, MNRAS, 292, 321